Somatodendritic orientation determines tDCS-induced neuromodulation of Purkinje cell activity in awake mice.

Carlos Andrés Sánchez-León[1,2], Guillermo Sánchez-Garrido Campos[1], Marta Fernández[3,4], Álvaro Sánchez-López[5], Javier F Medina[5] and Javier Márquez-Ruiz [1*]

[1]Department of Physiology, Anatomy and Cell Biology, Pablo de Olavide University, Ctra. de Utrera, km. 1, 41013, Seville, Spain. [2]Department of Neurology and Neurobiology, University of California Los Angeles, Los Angeles 90095, USA. [3] Department of Psychiatry, University of California Los Angeles, Los Angeles 90095, USA. [4] Department of Pharmacology, University of the Basque Country (UPV/EHU), Leioa 48940, Spain. [5]Department of Neuroscience, Baylor College of Medicine, Houston, TX, USA

Running title: tDCS neuromodulation of Purkinje cells *in vivo*

Acknowledgments: This work was supported by grants from the Spanish MINECO-FEDER (BFU2014-53820-P and BFU2017-89615-P) and FET European Union's Horizon 2020 research and innovation program (grant agreement No 101017716) to J.M-R and from the US National Institutes of Health (RF1MH114269) to J.F.M and J.M-R. C.A.S-L was in receipt of an FPU grant from the Spanish Government (FPU13/04858).

Keywords: cerebellum, non-invasive brain stimulation, transcranial electrical stimulation, transcranial direct-current stimulation, high-density recordings, juxtacellular

Corresponding author:
Javier Márquez-Ruiz, Ph.D.
Brain Stimulation translational Laboratory
Universidad Pablo de Olavide
Ctra. de Utrera, km. 1
41013-Sevilla, Spain
E-mail: jmarquez@upo.es
Phone: +34-954-978054

Declaration of interests: The authors declare no competing financial interests.

Abstract

Transcranial direct-current stimulation (tDCS) is a promising non-invasive neuromodulatory technique being proposed for treating neurologic disorders. However, there is a lack of knowledge about how externally applied currents affect neuronal spiking activity in cerebellar circuits *in vivo*. In this study, we observe a heterogeneous polarity modulation of the firing rate of Purkinje cells (PC) and non-PC in the mouse cerebellar cortex. Using a combination of juxtacellular labeling and high-density Neuropixels recordings, we demonstrate that the apparently heterogeneous effects of tDCS on PC activity can be fully explained by taking into account the somatodendritic orientation relative to the electric field. Our findings emphasize the importance of considering neuronal orientation and morphological aspects to increase the predictive power of tDCS computational models and optimize desired effects in basic and clinical human applications.

Introduction

Transcranial direct-current stimulation (tDCS) is a non-invasive brain stimulation technique consisting in the application of constant weak electric currents over the scalp for several minutes through strategically positioned electrodes[1,2]. In the last two decades, tDCS has demonstrated its feasibility to modulate cognitive, behavioral, and clinical traits[3] not only by its application over cerebral but also cerebellar cortex[4]. Nonetheless, together with tDCS growing popularity, also critical debates are increasing regarding the variability in results among studies[4,5]. This unreliability phenomenon can be explained by methodological differences and partly by the lack of knowledge about tDCS physiological mechanisms of action[6–8]. Understanding the neural basis underlying this variability becomes essential to develop new strategies to optimize the effects of tDCS in humans.

Animal models have played a key role in elucidating the mechanisms mediating tDCS effects, defining safety limits, inspiring new stimulation protocols, boosting brain function, validating computational models, and exploring new therapeutic applications[3,9]. *In vitro* studies have shown the significance of various neuronal features such as neuronal orientation and morphology[11–13] in the modulation of individual neurons' excitability. On the other hand, *in vivo* animal models have been successfully used to demonstrate the physiological effects of tES on spike timing[14,15], local field potential (LFP) oscillations[16,17], the correlation between LFP modulation and learning[17–20], as well as the involvement of other non-neuronal elements such as astrocytes or microglial cells[21,22]. *In vivo* experiments offer the opportunity to study the impact of tDCS on behaving brains, which allows for the measurement of the actual intracranial electric field induced by transcranial electrical stimulation (tES) and for testing the efficacy of tES protocols at both behavioral and physiological levels, providing insights into the underlying neuronal mechanisms. However, *in vivo* animal models usually have limited control over the applied electric fields in comparison with *in vitro* experiments and often lack the ability to identify the recorded neurons both functionally and morphologically. Therefore, in this context, it is necessary to identify different physiological aspects that could be responsible for the observed variability in tDCS effects and to use this information to inform existing realistic computational models in order to increase their predictive power.

Cerebellar tDCS has been demonstrated to modulate motor, cognitive, and emotional behaviors, relying on different cerebellar neural substrates, and has been proposed as a noninvasive neuromodulatory therapy for treating cerebellum-related disorders[23,24]. Interestingly, the cerebellum constitutes an excellent experimental model to study the impact of tDCS *in vivo*. Unlike the cerebral cortex, the cerebellum of rodents is highly convoluted, similar to that of humans in this aspect. Additionally, Purkinje cells (PCs) are electrophysiologically identifiable by complex and simple spike firing recording and represent the only output from cerebellar cortex[25–27]. In this study, we utilized the gyrated mice cerebellum to determine the significance of the Purkinje cell (PC) orientation on the final neuronal modulation induced by tDCS in awake mice. To investigate the effects of cerebellar tDCS on the cerebellar network output, we combined single-neuron extracellular recording of PCs in awake mice with juxtacellular recordings and subsequent staining of PC with neurobiotin under anesthesia. The morphological reconstruction of the recorded PCs allowed us to correlate their neuronal orientation with their response to tDCS. Finally, we utilized high-density Neuropixels recording system to demonstrate the relevance of neuronal orientation in awake mice, by simultaneously recording PCs with opposing orientations during

the application of tDCS.

Our work offers *in vivo* evidence that confirms the significance of neuronal orientation in relation to the generated electric field as a crucial factor in determining the modulation of firing rate exerted by tDCS, which explain the uneven effects observed across layers and neighboring regions. This result is essential for computational models and emphasizes the need to consider neuronal orientation when predicting final online tDCS effects in the cerebral and cerebellar cortices. These findings are useful in optimizing the desired tDCS effects in various cerebellum-related disorders[23,24].

Methods

Animal preparation.

Experiments were carried out on adult C57 male mice (n = 77) (University of Seville, Spain) weighting 28–35 g. All experimental procedures were carried out in accordance with European Union guidelines (2010/63/CE) and Spanish regulations (RD 53/2013) for the use of laboratory animals in chronic experiments. In addition, these experiments were submitted to and approved by the local Ethics Committee of the Pablo de Olavide University (Seville, Spain). Mice were prepared for simultaneous tES administration and electrophysiological recordings in the lateral (left) or vermis region of the cerebellar cortex in the head-restrained awake animal, following surgical procedures described previously[16]. In brief, animals were anesthetized with a ketamine–xylazine mixture (Ketaset, 100 mg/ml, Zoetis, NJ., USA; Rompun, 20 mg/ml, Bayer, Leverkusen, Germany), and a custom-made chlorinated silver ring electrode (2.5 mm inner ø, 3.5 mm outer ø) was placed over the skull centered on left crus I-II (AP = − 6 mm; L = +2 mm; relative to bregma[28]) (Fig. 1a) or on the cerebellar vermis (AP = − 6 mm; L = 0 mm; relative to bregma) and fixed with dental cement (DuraLay, Ill., USA). A 2 mm ø craniotomy was made centered in the ring and exposing the cerebellar cortex. The dura was left intact and protected with wax bone (Ethicon, Johnson & Johnson) until recordings begun. In addition, a silver wire electrode (ø: 381 µm, A-M Systems) was also implanted over the dura surface under the left parietal bone (AP = − 0.9 mm; L = + 3 mm; relative to bregma) as electrical reference for the electrophysiological recordings. Finally, a head-holding system was implanted, consisting of three bolts screwed to the skull and a bolt placed over the skull upside down and perpendicular to the frontal plane to allow for head fixation during the experiments. The holding system was cemented to the skull.

Single unit recordings.

Recording sessions began at least two days after surgery. The animals were placed over a treadmill with an infrared sensor for locomotion activity monitoring and the head was fixed to the recording table by means of the implanted head-holding system. Bone wax was removed with the aid of a surgical microscope (SMZ-140, Motic, Barcelona, Spain) and the cortical surface was carefully cleaned with super fine forceps (Dumont #5, FST, Heidelberg, Germany) and cotton swab without damaging the dura mater.

All single-cell recordings were carried out with an amplifier (BVC-700A, Dagan corporation, MN., USA) connected to a dual extracellular-intracellular headstage (8024, Dagan corporation, MN., USA; gain error ± 1%, noise 4.5 µV root mean square). The single-cell

recordings were performed with a glass micropipette (impedance 1–10 MΩ) filled with 3M NaCl, mounted on a micromanipulator (MO-10, Narishige, Tokyo, Japan). The electrode was slowly lowered at ~2 µm/s and spikes were detected based on visual (2002C and 2004C, Tektronix, OR., USA) and auditory (Audio monitor 3300, A-M Systems, WA., USA) cues. Once the spiking activity was detected, the micropipette tip was advanced slowly to properly isolate and identify single neuron activity in the recorded signal.

Juxtacellular labeling.

The procedure was similar to that of single-cell recordings except that the micropipette was filled with 2% Neurobiotin (SP-1120, Vector Laboratories, CA., USA) in 0.5 M NaCl, the tip was immersed in DiI (Vybrant DiI cell-labeling, V22885, Thermo Fisher Scientific, Mass., USA) and the impedance was periodically checked to assure that it was between 4–12 MΩ. With the headstage in extracellular mode and after single-cell activity was isolated, the micropipette tip was advanced until the negative spikes (extracellular recording) became positive spikes (juxtacellular recording) with an amplitude of at least 600 µV. Then, the headstage was switched to intracellular mode to juxtacellularly label the neuron following the method described by Pinault (Pinault, 1996). The firing rate of recorded neurons were modulated by passing positive current pulses (200 ms ON/OFF) at increasing intensities (1-10 nA) through the micropipette tip. After a delay of a few seconds, the electrical properties of the recorded neuron suddenly and significantly changed, increasing its firing rate and broadening the spike waveform. From this critical moment, pulse intensity was lowered to prevent cellular damage and the modulation was maintained from several seconds to minutes in order to fill the neuron with neurobiotin.

Neuropixels recording.

All Neuropixels recordings were performed using SpikeGLX (http://billkarsh.github.io/SpikeGLX/) on a computer connected to the PXIe acquisition module. Action potentials were band filtered between 0.3 and 10 kHz and sampled at 30 kHz whereas simultaneous LFPs were band filtered between 0.5 and 500 Hz and sampled at 2.5 kHz. Neuropixels's probe was coated with DiI lipophilic dye before insertion in the brain so a precise mark of the recording tract would be visible at confocal microscope. The probe was lowered in the coronal plane at 90 degrees from horizontal plane at ~2 µm/s until 4000 µm below cerebellar cortex surface. Neuropixels's probe was left to settle for 10 min to avoid drift during the recording.

Transcranial electrical stimulation.

The different protocols for transcranial currents were designed in Spike2 (Cambridge Electronic Design, CED, Cambridge, U.K.) and sent to a battery-driven linear stimulus isolator (WPI A395, Fl., USA) through an analog output from the acquisition board (CED micro1401-3). tES was applied between the ring-electrode and a reference electrode consisting of a rubber rectangular pad (6 cm^2) attached to the back of the mice and moisten with electrogel (Electro-Cap International, OH., USA). To measure the actual voltage changes elicited intracranially, sinusoid alternating current waves were delivered at amplitudes of ± 2, ± 20 and ± 200 µA (± 0.0426, ± 0.426 and ± 4.26 mA/cm^2) at 1 Hz and recorded in steps of 1 mm from cortical surface to 4 mm depth. To characterize the effects induced by tDCS, trials of 15 or 20 s pulses at 100, 200 and 300 µA anodal and cathodal tDCS (including 5 s ramp-in and 5 s ramp-out) were applied separated by 10 s of non-stimulation.

Histology.

To reconstruct the neurobiotin-labeled neurons, mice were deeply anesthetized with ketamine–xylazine mixture (Ketaset, 100 mg/ml; Rompun, 20 mg/ml) 15 min after juxtacellular labeling and perfused transcardially with 0.9% saline followed by 4% paraformaldehyde (Panreac, Barcelona, Spain) in PBS (0.1 M, pH ~7,4). The brains were removed and stored in 4% paraformaldehyde for 24 hours, cryoprotected in 30% sucrose in PBS the next 48 hours, and then cut into 50 µm coronal slices with a freezing microtome (CM1520, Leica, Wetzlar, Germany). After three washes with PBS-Triton X-100 1% (PBS-Tx, Sigma-Aldrich, Mo., USA), sections containing neurobiotin-labelled neurons were blocked with 10% Normal Donkey Serum (NDS, 566460, Merck, Darmstadt, Germany) in PBS-Tx and then incubated overnight at room temperature in darkness with Streptavidin 1:200 (Streptavidin DyLight 488 conjugated, Thermo Fisher Scientific) in PBS-Tx. After three washes with PBS, sections were mounted on glass slides and coverslipped using Dako fluorescence mounting medium (Agilent Technologies, Santa Clara, CA, USA). To determine recording regions across cerebellar tissue in Neuropixels recordings, the same process was carried out with the exception that after the three washes in PBS-Triton X-100 1%, slices were incubated for 3 min with Hoechst 33342 dye (Merck Millipore, Billerica, MA, USA) (2µg/ml) in PBS with 0.25% Triton X-100. For confocal imaging, an *in vivo* confocal microscope (A1R HD25, Nikon, Tokyo, Japan) was used. Z-series of optical sections (0.5 µm apart) were obtained using the sequential scanning mode.

Data analysis.

Data collection. Spike activity was recorded with a glass micropipette or a Neuropixels probe and sampled at 25 (CED micro1401-3) or 30 kHz (IMEC-PXIe) with an amplitude resolution of 12 and 10 bits, respectively. When necessary, LFP were sampled at 2.5 kHz and the remaining non-neuronal activities (tES, juxtacelullar injected currents and wheel movement) were sampled at 5 kHz.

Intracranial electric field analysis. The peak-to-peak amplitude (electric potential) of the LFP oscillations induced by tACS, were averaged for a given intensity and depth. For every intensity, the electric field strength (differences between potentials) was calculated by computing the difference in peak-to-peak values between two consecutive depths (1 mm in distance).

Single-cell activity. For glass micropipette recordings, only well isolated neurons, with high signal-to-noise ratios (at least 4 times the standard deviation of background noise) were considered for analysis. Spikes were detected offline in Spike2 (CED) and exported to MATLAB 2015a (MathWorks Inc., MA., USA) software for analysis. Trials where the mouse was running were removed from analysis. For spike detection, a “DC remove” process (time constant (s): 0.001-0.0004) was applied to reduce DC level drifts, and spikes were detected based on threshold-crossing algorithm of Spike2 software. After that, the DC remove process was carried out, and all spikes were visually confirmed and PC identified as such if complex spikes (CS) were observed and had at least a 10-40 ms pause in simple spikes (SS) after CS occurrence. For Neuropixel recordings, channels showing Purkinje cells, with CS followed by a SS silence, were manually selected on SpikeGLX (http://billkarsh.github.io/SpikeGLX/) and exported to analyze on Spike2 (CED, Cambridge, UK). Spike sorting was carried out using the Spike2 software and spikes with similar waveforms were grouped together in the same

templates. Putative Purkinje cell templates were subsequently curated to exclude contamination produced by other units. For this purpose, only periods where the template amplitude was stable were used, and events (spikes) with an amplitude deviation greater than one third of the average template amplitude were excluded. Additionally, the autocorrelogram was checked to discard contaminated templates with violations of the refractory period. Clusters corresponding to putative SS and CS were identified due to their waveform and their firing frequency (<3 Hz for CS and >50Hz for SS) and regularity, producing characteristic shoulders in the SS autocorrelogram. Finally, only those SS and CS from Purkinje cells unambiguously identified by the pause in their crosscorrelogram, were used for the analysis. Subsequently, each neuron was analyzed in MATLAB custom-made script. The 5 s window immediately before a stimulation ramp-in and immediately after a ramp-out were used for control and post-stimulation conditions, while the 5 s window immediately after the stimulation ramp reached the peak intensity was considered for tDCS condition. Averaged SS and CS waveforms, SS frequency, CS frequency and latency of the SS pause after CS were computed and analyzed for each condition. For SS firing rate analysis, all the trials with a given tDCS intensity and duration were averaged and then binned in 100 ms epochs in the five second windows computed for statistical analysis. For CS firing rate and latency of the SS pause after a CS analysis, the procedure was the same as before but instead of averaging between trials, we computed the different parameters for the 5 s windows (before, during and after tDCS) for every trial and the statistical comparisons were made between all the trials with a given tDCS intensity and time. Peristimulus time histograms showing the number of spikes per bin (bin size: 0.1 s for SS and 1 s for CS) were aligned with tDCS ramp-in, normalized and standardized (Z-score=X-μ/σ) with respect to the average frequency of the five seconds before anodal and cathodal tDCS ramp-in. To compare the strength of the modulation for the same neuron with different tDCS intensities and between neurons, the different parameters during tDCS were normalized by their values during control condition.

Neurobiotin-labeled neurons. Confocal images were processed in ImageJ (https://imagej.nih.gov/ij/) with the image processing package Fiji (http://fiji.sc/Fiji) to obtain a z-stack reconstruction of the neurobiotin-labelled neurons. The deviation of the somatodendritic axis with respect to the active electrode was calculated by measuring the angle between the neuronal axis and an imaginary line perpendicular to the active electrode.

Statistical analysis. Statistical comparison was inferred by repeated measures ANOVA (RM-ANOVA) using MATLAB 2015a. Neural activity parameters from each neuron were compared between the control, the tDCS and the post-stimulation periods. The non-parametric Friedman test was applied for comparisons when data did not permit normality assumption. The results are shown as mean ± SEM. Statistical significance was set at $p < 0.05$ in all cases.

Results

Electric field measurement in the cerebellar cortex

tDCS effects critically depend on the strength of the electric field imposed in the brain. To assess the actual electric field gradient imposed by tDCS in the cerebellar cortex in our experimental design, a group of mice (n = 9) was prepared for the chronic recording of LFPs in awake condition during simultaneous application of low-frequency transcranial

alternating-current stimulation (tACS) (1 Hz) at different intensities (± 2, ± 20, and ± 200 µA) (Fig. 1a). LFPs were sequentially recorded every 1 mm from the cortical surface to 4 mm depth (15º rostro-caudal insertion angle) (Fig. 1b). Figure 1 (c) shows the LFP recordings from a representative animal during simultaneous tACS (1 Hz, 10 s, ± 20 µA) at different depths, showing a decrease in voltage for deeper recordings. The estimation of the electric field strength (voltage difference) calculated at different depths (1, 2, 3 and 4 mm) and tACS intensities (± 2, circles; ± 20, squares; ± 200 µA, triangles) is represented in Fig. 1d (n = 9). Under the active electrode, the magnitude of the electric field decreased with depth in a logarithmic manner for the three tested intensities (R = 0.98, 0.96 and 0.95 for ± 2, ± 20, and ± 200 µA, respectively; data is presented with logarithmic abscissa axis for visual facilitation, Fig. 1d). With this data, the electric field imposed by tACS at different depths and intensities tested in our experiments was interpolated. A polynomial surface (degree 2 for depth and degree 2 for intensity axis) was fitted on the electric field values and then the coefficients (with 95% confidence bounds) were extracted from the linear model. Considering the most superficial (0.3 mm) and the deepest (2.3 mm) recorded neurons, we could expect electric field values between 60.1, 92.9 and 125.7 V/m (at 0.3 mm for 100, 200 and 300 µA, respectively) and 5.9, 20.2 and 34.6 V/m (at 2.3 mm for 100, 200 and 300 µA, respectively) at the recording places. These values are in line with *in vitro* and other *in vivo* animal studies showing modulation of neuronal firing rate under similar current densities.

tDCS modulates Purkinje cell activity in awake mice in a heterogeneous manner

To understand how tDCS modulates neuronal firing behavior at a single-cell level, we performed single-cell recordings in awake mice using glass micropipettes. We first focused on the potential impact of exogenous electric fields on PC firing rate. Unlike other cerebellar neuronal types, PC can be electrophysiologically identified by the presence of SS and CS[25,26] followed by a brief SS silence (Fig. 2a,b and Supplementary Fig. 1a-d). To determine the online effects of exogenous electric field application on PC firing rate and avoid long-term plasticity mechanisms, short pulses of tDCS (15 s including 5 s ramp-in and 5 s ramp-out, ± 200 µA) separated by non-stimulating periods (10 s) were applied. Figure 2a-f shows two representative PCs and their firing behavior during simultaneous tDCS (Fig. 2c-f). As observed in the Z-score-transformed average firing rate, the SS firing rate of some recorded PCs significantly increased during anodal and decreased during cathodal tDCS (Fig. 2c,e) whereas the opposite effects were observed in other recorded neurons decreasing the SS firing rate during anodal and increasing during cathodal (Fig. 2d,f) (Paired Student's t-test, $p < 0.01$). Furthermore, we could observe a significant rebound effect when tDCS was switched off for some of the neurons (Fig. 2d,f). A total of 25 identified PCs were recorded in crus I-II region (Fig. 2g,h) in awake mice (n = 24 animals). The impact of anodal and cathodal tDCS on the SS firing rate showed significant differences (filled circles) for 19 out of 25 individual PCs recorded (n = 25, RM-ANOVA or Friedman tests, $p < 0.05$) (Fig. 2g and Supplementary Fig. 2a,b). The data distribution was fitted by a linear model (R = 0.67, $p < 0.0002$) and most of PCs increased their firing rate with anodal stimulation and decreased with cathodal stimulation or vice versa.

No differences were observed in the waveform of recorded SS nor CS during anodal nor cathodal tDCS with respect to control condition (Supplementary Fig. 1a-d; black trace). No significant changes were observed in the CS firing rate during tDCS (Supplementary Fig. 1e-h)

(n = 25, Paired Student's t-test) except for one of the recorded PCs. The impact of anodal and cathodal tDCS in CS firing rate and SS silence for all the individual PCs recorded in crus I-II of awake animals shows scarce significant changes in CS firing rate or SS silence (Supplementary Fig. 1i,j).

From these first results, we can conclude that PCs, constituting the only output from cerebellar cortex, 1) are modulated by tDCS for the electric field gradient applied in this experiment and 2) this modulatory effect is heterogeneous across PC population.

Non-Purkinje cell activity is also modulated by tDCS in awake mice

Beyond the inhibitory PCs, the cerebellar cortex neuronal network is constituted by excitatory (granular cell) and inhibitory (Golgi cell, Lugaro cells, basket cells and stellate cells) neurons responsible to determine spatio-temporal PC output[27]. The modulatory effects of tDCS on the activity of these non-PC neurons could be important in feed-forward, feedback, and lateral inhibition processes underlying cerebellar function. Unlike PCs, these neurons do not show typical SS and CS in the neuronal recording and cannot be electrophysiologically identified. For analysis purposes, we decided to include these neurons in “non-PC” group. The same tDCS protocol previously used with PCs was applied to determine the online effects of exogenous electric field application on non-PC firing rate.

Fig. 3a-f shows two representative non-PCs and their firing behavior during simultaneous tDCS. As observed in the Z-score-transformed average, the firing rate of some recorded non-PCs significantly increased during anodal and decreased during cathodal tDCS (Fig. 3c,d) whereas different effects were observed in other recorded neurons increasing during cathodal (Fig. 3e,f) (Paired Student's t-test, $p < 0.05$). Furthermore, similar to previously observed in PC, we could observe a significant rebound effect when tDCS was switched off for some of the neurons (Fig. 3c-f). A total of 50 non-PCs were recorded in crus I-II region (Fig. 3g-i) in awake mice (n = 24 animals). The impact of anodal and cathodal tDCS in the firing rate showed significant differences (filled circles) for 36 of out of 50 individual non-PCs recorded (n = 50, RM-ANOVA or Friedman tests, $p < 0.05$) (Fig. 3g Supplementary Fig. 2c,d). The data distribution was fitted by a linear model ($R = 0.56$, $p < 0.0001$) and was found to have higher dispersion than the PC data (Fig. 2g). No differences were observed in the waveform of recorded spikes during anodal nor cathodal tDCS with respect to control condition.

These results allow us to conclude that not only PC, but non-PC implicated in the spatio-temporal response of PCs are modulated during tDCS in a heterogeneous way.

Purkinje cell orientation in cerebellar cortex explain tDCS heterogeneous modulation in anesthetized mice.

Given the large heterogeneity observed in the responses of the recorded cerebellar neurons to tDCS and considering the anatomical complexity of the highly convoluted cerebellar cortex, we wondered if the somatodendritic axis orientation of the cerebellar neurons could partially explain this variability, as suggested by previous *in vitro* studies [12,13,29]. For this purpose, we decided 1) to record in the cerebellar vermis region with PC oppositely oriented in adjacent cortical layers and 2) label some of the recorded PC with neurobiotin after

electrophysiological characterization.

A total of 56 neurons (31 identified PCs and 25 non-PCs) were recorded in the vermis of 27 anesthetized mice (Fig. 4a) during anodal and cathodal tDCS (±200 µA). The impact of anodal and cathodal tDCS on the firing rate showed significant differences (filled circles) in 27 out 31 PCs (Fig. 4b) and in 17 out 25 recorded non-PCs (Fig. 4c) during anodal and cathodal tDCS (n = 31 PCs and 25 non-PCs, RM-ANOVA or Friedman tests, $p < 0.05$) (Supplementary Fig. 3). As we can see, the effects of tDCS on PC firing rate adjusts to a linear regression (slope -0.57, $R = 0.7$, $p < 0.0001$) (Fig. 4b), whereas the effects were scattered on non-PC (slope -0.19, $R = 0.35$, $p < 0.0875$) (Fig. 4c). This result suggests that in the vermis there is a consistent polarity-dependent modulation for PC, where anodal and cathodal modulate firing rate in opposite ways. However, this effect is not observed in non-PC group. The findings remained consistent even when we tested the same neurons with greater (±300 µA) and lesser (±100 µA) current intensities (Supplementary Fig. 2a-f). From this section we can conclude that 1) tDCS in vermis of anesthetized mice modulates PC and non-PC in a heterogeneous way, 2) tDCS in vermis modulate more PC than in Crus I-II and 3) PCs in vermis show a polarity and intensity-dependent modulation.

To test if the opposite modulation of PCs by anodal and cathodal stimulation could be related to the opposite somatodendritic orientation of these neurons with respect to the electric field a total of 8 recorded PCs in 8 animals were successfully stained with neurobiotin using juxtacellular microinjection in the anesthetized mice (either in crus I-II or vermis). For that, once PC response to tDCS was characterized, brief (200 ms on-off) low-current (1-10 nA) electrical pulses were passed through the tip of the recording micropipette loaded with neurobiotin until the firing of the neuron was clearly entrained with the applied current pulses. Labeled PCs were reconstructed with confocal microscopy and the deviation of the somatodendritic axis from the imaginary line perpendicular to the active electrode was calculated (Fig. 5a; θ angle). Figure 5a-d shows representative PCs with different θ angle together with Z-score-transformed average PSTH (bin size: 0.1 s) of the spiking activity and statistical comparison of the firing rate before, during and after anodal (red) or cathodal (blue) tDCS (Friedman test, $p < 0.05$). Thus, when θ was close to 0º (the somatodendritic axis was pointing toward the active electrode, Fig. 5a) anodal tDCS tended to increase the firing rate and cathodal reliably decreased it, whereas when θ was close to 90º (the axis was more parallel to the active electrode) (Fig. 5b) the modulatory effect was absent. However, when θ value was close to 180º (the somatodendritic axis was pointing away from the electrode) (Fig. 5c), the opposite modulation was observed, with anodal decreasing and cathodal increasing the firing rate, and again the effect was more subtle for neurons with θ close to 270º (more parallel orientations) (Fig. 5d). Figure 5e summarizes the relationship between the θ angle and tDCS modulation of all labeled neurons. The figure represents the normalized firing rate modulation ([firing rate during tDCS/firing rate before tDCS]*100; length of the arrow) and θ angle value for each recorded neuron during anodal (Fig. 5e, at left) and cathodal (Fig. 5e, at right) tDCS. Figure 5f represents the relationship between the normalized firing rate modulation of each individual neuron with respect to its corresponding θ angle for anodal (red line) or cathodal (blue line) tDCS. The impact of tDCS in the firing rate of PC was higher for those neurons with θ values close to 0º and 180º for anodal and cathodal currents acting in a polarity-dependent manner. These results corroborate that the somatodendritic axis orientation plays a critical role in explaining tDCS heterogeneous modulation of individual PCs in anesthetized mice.

Purkinje cell orientation determines polarity of modulation in the awake mice.

To examine whether the effects of PC orientation that we observed in anesthetized mice can be extended to the more clinically relevant awake state, we took advantage of Neuropixels technology, a fully integrated silicon probe for high-density stable recording of neural activity allowing for the simultaneous recording of dozens of neurons. For that, we prepared 7 additional mice for chronic multiunitary neuronal recording during simultaneous tDCS. Neuropixels probes were coated with lipophilic dyes (DiI) for the posterior histological reconstruction of the recording place. A total of 22 identified PCs were recorded in the vermis of the 7 recorded animals from which only 12 were unequivocally isolated for analysis during tDCS. Figure 6a illustrates probe location marked with DiI in the cerebellar vermis of a representative animal. The estimated location for each probe contact in the region of interest where two different PCs with the somatodendritic axis pointing toward and away from the active electrode recorded at Ch#55 and Ch#42, respectively (Fig. 6b), are shown together with Z-score-transformed average PSTH (bin size: 0.1 s for SS) of the spontaneous SS before, during and after anodal (red trace) and cathodal (blue trace) tDCS (Fig. 6c). Remarkably, we found that simultaneously recorded PCs in oppositely oriented PC layers exhibit opposite effects in presence of anodal or cathodal tDCS in awake mice. The anatomical location of all the individually recorded PCs and the impact of anodal and cathodal tDCS in their firing rates are presented in figure 6d. As we can see in Fig. 6e, PC modulation adjusts to a linear regression, suggesting a polarity-dependent modulation where anodal and cathodal modulate firing rate in opposite ways. In addition, PCs located in vermis showed a better polarity-dependent modulation than in crus I-II (Fig. 2g), as suggested by the higher slope and R values in awake (Fig. 6e) but also anesthetized (Fig. 4b) recordings in vermis. This experiment corroborates in the awake animal and in simultaneously recorded PC that 1) a given tDCS polarity (either anodal or cathodal) can modulate distinct neurons in opposite ways at the same time, increasing and decreasing their firing rates, and 2) the somatodendritic axis orientation of PCs is a key factor predicting tDCS modulation.

Discussion

In this study, we used *in vivo* unitary recordings from cerebellar neurons to show tDCS capability to modulate neuronal activity in awake mice. After calculating the electric field gradient imposed in the cerebellum by transcranial stimulation, we proved that, under these conditions, most of the recorded PCs and non-PCs were modulated by tDCS, either with anodal, cathodal or both polarities. The observed effect was heterogenous, with anodal (but also cathodal) increasing the firing rate in some neurons but decreasing it in others. Nonetheless, we observed a clear polarity-dependent modulation. The heterogeneity observed was largely explained by the somatodendritic axis orientation with respect to the active electrode, as showed by matching *in vivo* electrophysiological recordings together with neurobiotin-labeling of individual neurons in anesthetized and Neuropixels high-density recordings in awake animals under tDCS.

Measurement of the electric field in the cerebellar cortex of the mice

tDCS neuromodulatory effects strongly depend on the magnitude of electric fields imposed in the brain. This magnitude is directly related to the electric current intensity and the size of the electrodes (i.e., current density) but also to the shunt produced by the tissue between the electrodes and the brain[30,31]. Thus, around 60% of the applied current is shunted by the skin and around 20% is attenuated by the skull [32,33]. For this reason, if we want to compare our results with human studies, we must address the strength of the actual electric field gradient generated in the brain in our preparation. Usually, human studies rely on computational models using realistic head models to predict how electric currents diffuse across the brain in different tDCS montages [34–36], nonetheless, animal studies offer an opportunity to characterize the actual electric field imposed in the region of interest for the experimental design[14,15,32,37,38]. As expected from cerebellar modelling studies[36,39]and observed *in vitro*[40] and *in vivo*[15], the current flow in the cerebellum is largely uniform in direction, with the highest electric field values observed in the first millimeter of the cortex (64.8, 6.9 and 0.97 V/m for 200, 20 and 2 µA, respectively) and decaying with distance in a logarithmic manner.

Impact of tDCS on single neurons in the awake mice

To understand basic mechanisms by which tDCS modulates neuronal activity, we performed single neuron recordings in awake mice to rule out any possible interaction of the anesthetic with tDCS effects and looking for the most physiologically similar conditions to human experiments. We observed a robust firing rate modulation during tDCS, with over 72% of the recorded neurons being modulated. This modulation was also polarity-dependent, in agreement with previous *in vivo* work from anesthetized rat cerebral[32,41] and cerebellar[15] cortices. The observed modulatory effects were always heterogeneous among different neurons, regardless of the polarity and intensity tested. Some neurons increased or decreased their firing rate under anodal or cathodal stimulation, respectively, while others behaved in the opposite manner. Furthermore, in our study the firing rate changes elicited by tDCS suggest a polarizing effect of the applied currents, which will result from changes in the membrane resting potential[10,11,32,35]. As we can see in most of the z-scored histograms (Fig. 2,3,5 and 6), the firing rate is modulated along time in accordance with transcranial current dynamics (i.e., variable in ramp-in and ramp-out periods and stable during the 5 or 10 s at maximum intensity), except for a rebound effect observed after current termination (also observed by Asan et al.[15]). Nonetheless, we can expect a combined effect of modulations on neuronal firing rate. The electric field gradient imposed by tDCS can directly modulates neuronal firing rate by changes in membrane resting potential, but also indirectly affects the firing rate through changes in network activity from other neurons that synapse on the recorded neuron. In fact, these synaptic changes could explain the rebound effect since these synapses could undergo a short-term plasticity process[10,42–44] and at this point there are no external currents being applied.

Additionally, we analyzed different neuronal activity parameters with physiological relevance. We measured CS firing rate and the latency of the SS silence after a complex spike, two parameters highly relevant for cerebellar learning function[45]. These two parameters have been recently proposed to be modified during tDCS in a modeling study using multicompartment models of PCs, deep cerebellar nuclei and granule cell[46]. Nevertheless, even when we observed a heterogeneity in the modulation of these parameters similar to SS

firing rate and a statistically significant modulation for some few neurons, there were no significant differences in most of the analyzed neurons. The low firing rate of CS and the limited number of trials used in the *in vivo* recordings could be behind the lack of more statistically significant results. Furthermore, our results demonstrate *in vivo* how tDCS can modulate the firing rate of both PC and non-PC populations, a robust result contradicting the previously mentioned multicompartment modeling study[46] predicting that only PC population, and no other studied cerebellar neurons, are likely to experience a change in tonic firing under tDCS. It could be argued that modeling conditions, mimicking lower electric fields used in humans (~1-1.5 V/m) could be enough to explain these differences. Nevertheless, based on the anatomical location of some of our non-PC recorded, together with the empirical measurement of the imposed electric-field, a clear modulatory effect of the firing rate (an increase of 137.6% for anodal and decrease of 61.7% for cathodal) at relatively low electric field strength (5.9 V/m; depth: 2.3 mm; tDCS intensity: 100 µA) was observed, so we could expect a similar PC and non-PC modulation under electric fields applied in human studies.

Importance of somatodendritic axis orientation on tDCS effects

Trying to understand the underlying basis of the observed heterogeneity in firing rate modulation, we speculated that the orientation of the PC with respect to the electric field could explain some of this variability. Previous *in vitro* and modelling studies highlighted the relevance of different neuronal features underlying tDCS effects, such as the orientation of somatodendritic axes with respect to the electrical field[47], the neuronal morphology[12] or the axonal orientation[13]. To test this hypothesis *in vivo*, we took advantage of the highly convoluted mice cerebellum and labeled PC from different areas with different neuronal orientations (crusI-II in the lateral cerebellum and vermis). First, we observed a greater proportion of modulated PCs and polarity-dependent responses in vermis than in crus I-II of awake mice. However, non-PC modulation did not differ much between the recording regions, suggesting a role for the PC neuronal orientation and morphology regarding tDCS modulation. When we labeled some of these PCs with neurobiotin we could clearly observe that the firing rate modulation highly depends on the somatodendritic axis orientation with respect to the active electrode (Fig. 5). Similar results were observed from *ex vivo* experiments performed in isolated turtle cerebellum[40,48] where anodal stimulation predominantly excited the cell bodies of PC (also stellate cells) when their dendritic trees were oriented toward the active electrode, corroborating that the major determinant of modulation (at least for cerebellar PC neurons) was the orientation of the dendritic tree. Finally, the relevance of PC orientation in the final impact of tDCS was demonstrated in the awake animals by means of high-density neuronal recordings showing opposite firing rate modulation in oppositely oriented adjacent PC. As a result, the final macroscopic cerebellar tDCS effects will depend on the net modulation of different neuronal components in the stimulated network, which will be strongly determined by the orientation of the Purkinje cells in the stimulated folia. It's also important to note that most tDCS studies performed in humans focus on the long-term effects induced after prolonged tDCS, which can be different from the online effects observed during stimulation[16].

In conclusion, we found that tDCS can modulate the firing rate of cerebellar cortex neurons in mice in a polarity-dependent manner, and this modulation is highly dependent on neuronal

orientation. Our findings emphasize the importance of considering neuronal orientation and morphology aspects of PC and non-PC when applying transcranial stimulation, at least in the cerebellum. Considering these aspects would be crucial to increase the predictive power of tDCS computational models and optimize desired effects in basic and clinical human applications.

Author contributions

C.A.S-L and J.M-R conceived the original idea and designed the experiments. C.A.S-L, G.S-G.C, M.F and J.M-R performed the experiments and the data analysis. C.A.S-L and J.M-R wrote the paper. A.S-L and J.F.M assisted in the experimental design and in the interpretation of the results. All the authors contributed to the final edition of the manuscript.

References

1. Nitsche, M. & Paulus, W. Excitability changes induced in the human motor cortex by weak transcranial direct current stimulation. *J. Physiol.* **527**, 633–9 (2000).

2. Woods, A. J. *et al.* A technical guide to tDCS, and related non-invasive brain stimulation tools. *Clin. Neurophysiol.* **127**, 1031–1048 (2016).

3. Stagg, C. J., Antal, A. & Nitsche, M. A. Physiology of Transcranial Direct Current Stimulation. *J. ECT* **34**, 144–152 (2018).

4. Horvath, J. C., Forte, J. D. & Carter, O. Evidence that transcranial direct current stimulation (tDCS) generates little-to-no reliable neurophysiologic effect beyond MEP amplitude modulation in healthy human subjects: A systematic review. *Neuropsychologia* **66**, 213–236 (2015).

5. Antal, A., Keeser, D., Priori, A., Padberg, F. & Nitsche, M. A. Conceptual and Procedural Shortcomings of the Systematic Review 'Evidence That Transcranial Direct Current Stimulation (tDCS) Generates Little-to-no Reliable Neurophysiologic Effect Beyond MEP Amplitude Modulation in Healthy Human Subjects: A Systematic Review' by Horvath and Co-workers. *Brain Stimul.* **8**, 846–849 (2015).

6. Horvath, J. C., Carter, O. & Forte, J. D. No significant effect of transcranial direct current stimulation (tDCS) found on simple motor reaction time comparing 15 different simulation protocols. *Neuropsychologia* **91**, 544–552 (2016).

7. Liu, A. *et al.* Immediate neurophysiological effects of transcranial electrical stimulation. *Nat. Commun.* **9**, 5092 (2018).

8. Polanía, R., Nitsche, M. A. & Ruff, C. C. Studying and modifying brain function with non-invasive brain stimulation. *Nat. Neurosci.* **21**, 174–187 (2018).

9. Sánchez-León, C. A., Ammann, C., Medina, J. F. & Márquez-Ruiz, J. Using Animal Models

to Improve the Design and Application of Transcranial Electrical Stimulation in Humans. 125–135 (2018) doi:10.1007/s40473-018-0149-6.

10. Farahani, F., Kronberg, G., FallahRad, M., Oviedo, H. V. & Parra, L. C. Effects of direct current stimulation on synaptic plasticity in a single neuron. *Brain Stimul.* **14**, 588–597 (2021).

11. Bikson, M. *et al.* Effect of uniform extracellular DC electric fields on excitability in rat hippocampal slices in vitro. *J. Physiol.* **557**, 175–190 (2004).

12. Radman, T., Ramos, R., Brumberg, J. & Bikson, M. Role of Cortical Cell Type and Morphology in Sub- and Suprathreshold Uniform Electric Field Stimulation. *Brain Stimul.* **2**, 215–228 (2009).

13. Kabakov, A. Y., Muller, P. A., Pascual-Leone, A., Jensen, F. E. & Rotenberg, A. Contribution of axonal orientation to pathway-dependent modulation of excitatory transmission by direct current stimulation in isolated rat hippocampus. *J. Neurophysiol.* **107**, 1881–1889 (2012).

14. Huang, W. A. *et al.* Transcranial alternating current stimulation entrains alpha oscillations by preferential phase synchronization of fast-spiking cortical neurons to stimulation waveform. *Nat. Commun.* **12**, (2021).

15. Asan, A. S., Lang, E. J. & Sahin, M. Entrainment of cerebellar purkinje cells with directional AC electric fields in anesthetized rats. *Brain Stimul.* **13**, 1548–1558 (2020).

16. Sánchez-León, C. A. *et al.* Immediate and after effects of transcranial direct-current stimulation in the mouse primary somatosensory cortex. *Sci. Reports 2021 111* **11**, 1–15 (2021).

17. Krause, M. R. *et al.* Transcranial Direct Current Stimulation Facilitates Associative Learning and Alters Functional Connectivity in the Primate Brain. *Curr. Biol.* **27**, 3086-3096.e3 (2017).

18. Márquez-Ruiz, J. *et al.* Transcranial direct-current stimulation modulates synaptic mechanisms involved in associative learning in behaving rabbits. *Proc. Natl. Acad. Sci.* **109**, 6710–6715 (2012).

19. Reinhart, R. M. G., Woodman, G. F. & Posner, M. I. Enhancing long-term memory with stimulation tunes visual attention in one trial. *Proc. Natl. Acad. Sci. U. S. A.* **112**, 625–630 (2015).

20. Reinhart, R. M. G., Zhu, J., Park, S. & Woodman, G. F. Medial-Frontal Stimulation Enhances Learning in Schizophrenia by Restoring Prediction Error Signaling. *J. Neurosci.* **35**, 12232–12240 (2015).

21. Monai, H. *et al.* Calcium imaging reveals glial involvement in transcranial direct current stimulation-induced plasticity in mouse brain. *Nat. Commun.* **7**, 1–10 (2016).

22. Mishima, T. *et al.* Transcranial direct current stimulation (tDCS) induces adrenergic receptor-dependent microglial morphological changes in mice. *eNeuro* **6**, 1–12 (2019).

23. Manto, M. *et al.* Consensus Paper: Novel Directions and Next Steps of Non-invasive Brain Stimulation of the Cerebellum in Health and Disease. *Cerebellum 2021* 1–31 (2021) doi:10.1007/S12311-021-01344-6.

24. Grimaldi, G. *et al.* Cerebellar Transcranial Direct Current Stimulation (ctDCS): A Novel Approach to Understanding Cerebellar Function in Health and Disease. *Neuroscientist* **22**, 83–97 (2016).

25. Davie, J. T., Clark, B. A. & Häusser, M. The origin of the complex spike in cerebellar Purkinje cells. *J. Neurosci.* **28**, 7599–7609 (2008).

26. Raman, I. M. & Bean, B. P. Resurgent Sodium Current and Action Potential Formation in Dissociated Cerebellar Purkinje Neurons. *J. Neurosci.* **17**, 4517 (1997).

27. Prestori, F., Mapelli, L. & D'Angelo, E. Diverse Neuron Properties and Complex Network Dynamics in the Cerebellar Cortical Inhibitory Circuit. *Front. Mol. Neurosci.* **12**, (2019).

28. Paxinos, G. & Franklin, K. B. J. *The mouse brain in stereotaxic coordinates, Second edition*. (2004).

29. Bikson, M., Reato, D. & Rahman, A. Cellular and Network Effects of Transcranial Direct Current Stimulation. *Transcranial Brain Stimul.* 55–92 (2012) doi:10.1201/b14174-5.

30. Opitz, A., Falchier, A., Linn, G. S., Milham, M. P. & Schroeder, C. E. Limitations of ex vivo measurements for in vivo neuroscience. *Proc. Natl. Acad. Sci.* **114**, 5243–5246 (2017).

31. Gomez-Tames, J. *et al.* Group-level and functional-region analysis of electric-field shape during cerebellar transcranial direct current stimulation with different electrode montages. *J. Neural Eng.* **16**, 036001 (2019).

32. Vöröslakos, M. *et al.* Direct effects of transcranial electric stimulation on brain circuits in rats and humans. *Nat. Commun.* **9**, 483 (2018).

33. Liu, A. *et al.* Immediate neurophysiological effects of transcranial electrical stimulation. *Nature Communications* vol. 9 at https://doi.org/10.1038/s41467-018-07233-7 (2018).

34. Ruffini, G., Fox, M. D., Ripolles, O., Miranda, P. C. & Pascual-Leone, A. Optimization of multifocal transcranial current stimulation for weighted cortical pattern targeting from realistic modeling of electric fields. *Neuroimage* **89**, 216–225 (2014).

35. Huang, Y., Datta, A., Bikson, M. & Parra, L. C. Realistic volumetric-approach to simulate transcranial electric stimulation—ROAST—a fully automated open-source pipeline. *J. Neural Eng.* **16**, 056006 (2019).

36. Parazzini, M. *et al.* Modelling the electric field and the current density generated by cerebellar transcranial DC stimulation in humans. *Clin. Neurophysiol.* **125**, 577–584 (2014).

37. Opitz, A. *et al.* Spatiotemporal structure of intracranial electric fields induced by transcranial electric stimulation in humans and nonhuman primates. *Sci. Rep.* **6**, 1–11 (2016).

38. Johnson, L. *et al.* Dose-dependent effects of transcranial alternating current

stimulation on spike timing in awake nonhuman primates. *Sci. Adv.* **6**, 1–8 (2020).

39. Rahman, A., Toshev, P. K. & Bikson, M. Polarizing cerebellar neurons with transcranial Direct Current Stimulation. *Clin. Neurophysiol. J.* **125**, 435–438 (2014).

40. Chan, C. Y. & Nicholson, C. Modulation by applied electric fields of purkinje and stellate cell activity in the in the isolated turtle cerebellum. *J. Physiol.* **371**, 89–114 (1986).

41. Bindman, L. J., Lippold, O. C. J. & Redfearn, J. W. T. The action of brief polarizing currents on the cerebral cortex of the rat (1) during current flow and (2) in the production of long-lasting after-effects. *J. Physiol.* **172**, 369–382 (1964).

42. Cirillo, G. *et al.* Neurobiological after-effects of non-invasive brain stimulation. *Brain Stimul.* **10**, 1–18 (2017).

43. Kronberg, G., Bridi, M., Abel, T., Bikson, M. & Parra, L. C. Direct Current Stimulation Modulates LTP and LTD: Activity Dependence and Dendritic Effects. *Brain Stimul.* **10**, 51–58 (2017).

44. Kronberg, G., Rahman, A., Sharma, M., Bikson, M. & Parra, L. C. Direct current stimulation boosts hebbian plasticity in vitro. *Brain Stimul.* **13**, 287–301 (2020).

45. Streng, M. L., Popa, L. S. & Ebner, T. J. Complex Spike Wars: a New Hope. *Cerebellum* **17**, 735–746 (2018).

46. Zhang, X., Hancock, R. & Santaniello, S. Transcranial direct current stimulation of cerebellum alters spiking precision in cerebellar cortex: A modeling study of cellular responses. *PLoS Comput. Biol.* **17**, (2021).

47. Rahman, A. *et al.* Cellular effects of acute direct current stimulation: Somatic and synaptic terminal effects. *J. Physiol.* **591**, 2563–2578 (2013).

48. Chan, C. Y., Hounsgaard, J. & Nicholson, C. Effects of electric fields on transmembrane potential and excitability of turtle cerebellar Purkinje cells in vitro. *J. Physiol.* **402**, 751–771 (1988).

Figures

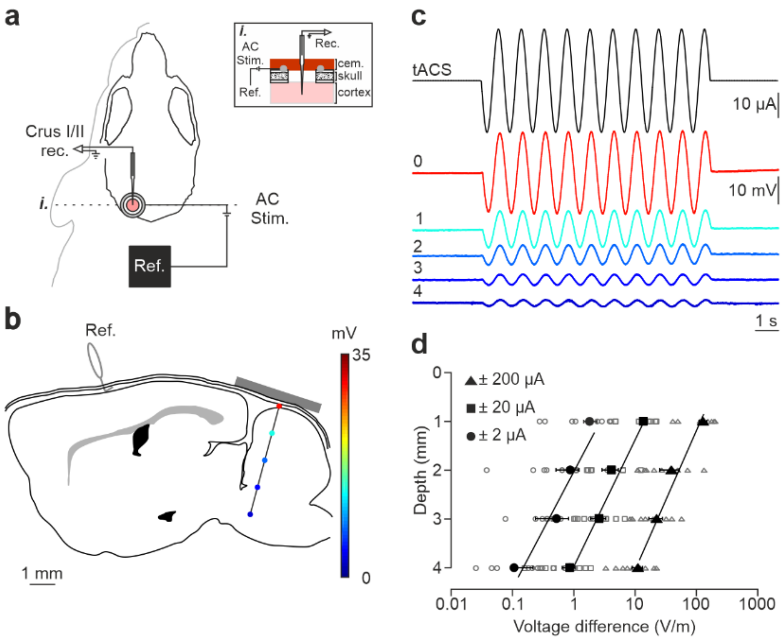

Fig. 1 Intracranial electric fields induced by Cb-tACS. **a** Experimental design for *in vivo* electrophysiology in crus I-II cerebellar region in awake mice showing silver-ring active and reference (Ref.) electrode locations for transcranial alternating current stimulation (tACS). Inset (*i.*) shows a schematic sagittal view of the recording site. **b** Schematic representation of a sagittal section of the brain showing the reference (Ref.) and active electrodes location (gray bar) and a representative track in the lateral cerebellum highlighting the depths where the electric field was measured (color dots). **c** tACS stimulation (top trace) applied over the scalp and exemplary recording of the actual field potentials generated at different depths (from 0 to 4 mm) in a representative animal. The traces were overlapped to facilitate amplitude comparison. **d** Average (filled symbols) and individual (empty symbols) electric field strength recorded at different depths for ± 2 (circles), ± 20 (squares) and ± 200 µA (triangles) tACS.

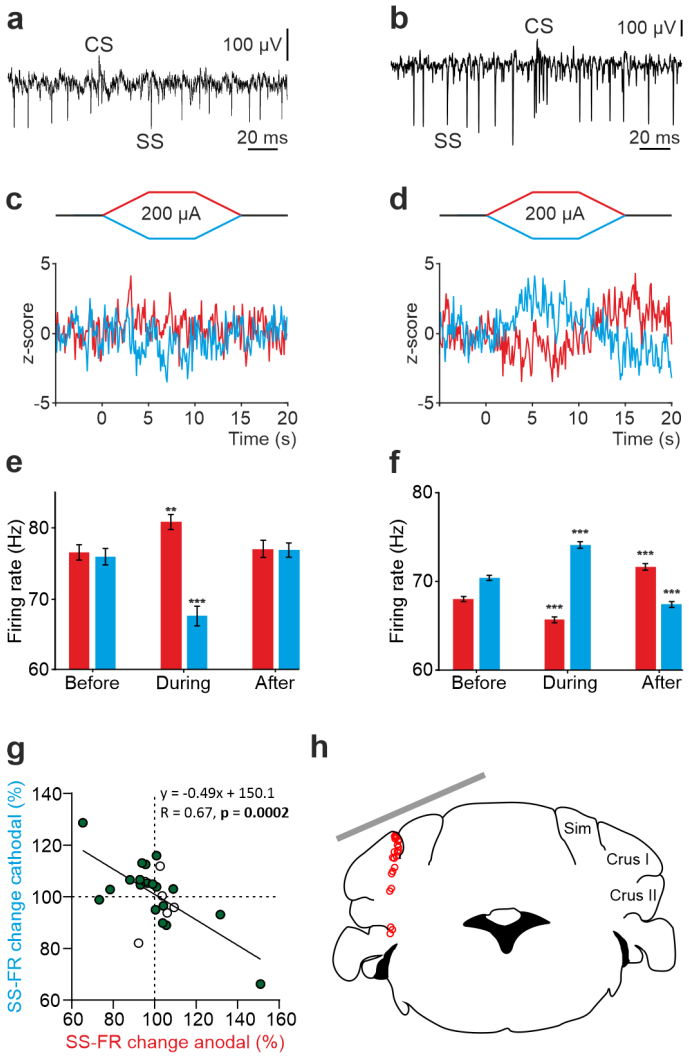

Fig. 2 tDCS modulation of PC activity in the awake mice. a, b Recording of spontaneous firing activity of two PCs showing the presence of SS and CS. **c,d** Z-score-transformed average PSTH (bin size: 0.1 s) of the spontaneous SS activity before, during and after anodal (red trace) or cathodal (blue trace) tDCS. **e,f** Statistical comparison of the SS firing rate between 5 s windows before, during and after tDCS (RM-ANOVA or Friedman tests, $p < 0.05$). Error bars represent SEM. $^{**}p < 0.01$; $^{***}p < 0.001$. **g** Modulation of SS (p) of individual neurons (circles) during anodal (red) and cathodal (blue) tDCS. Filled circles represent statistically significant modulation during tDCS (n = 25, RM-ANOVA or Friedman tests, $p < 0.05$). **h** Schematic representation of the recording sites and active electrode location (gray bar) during tDCS.

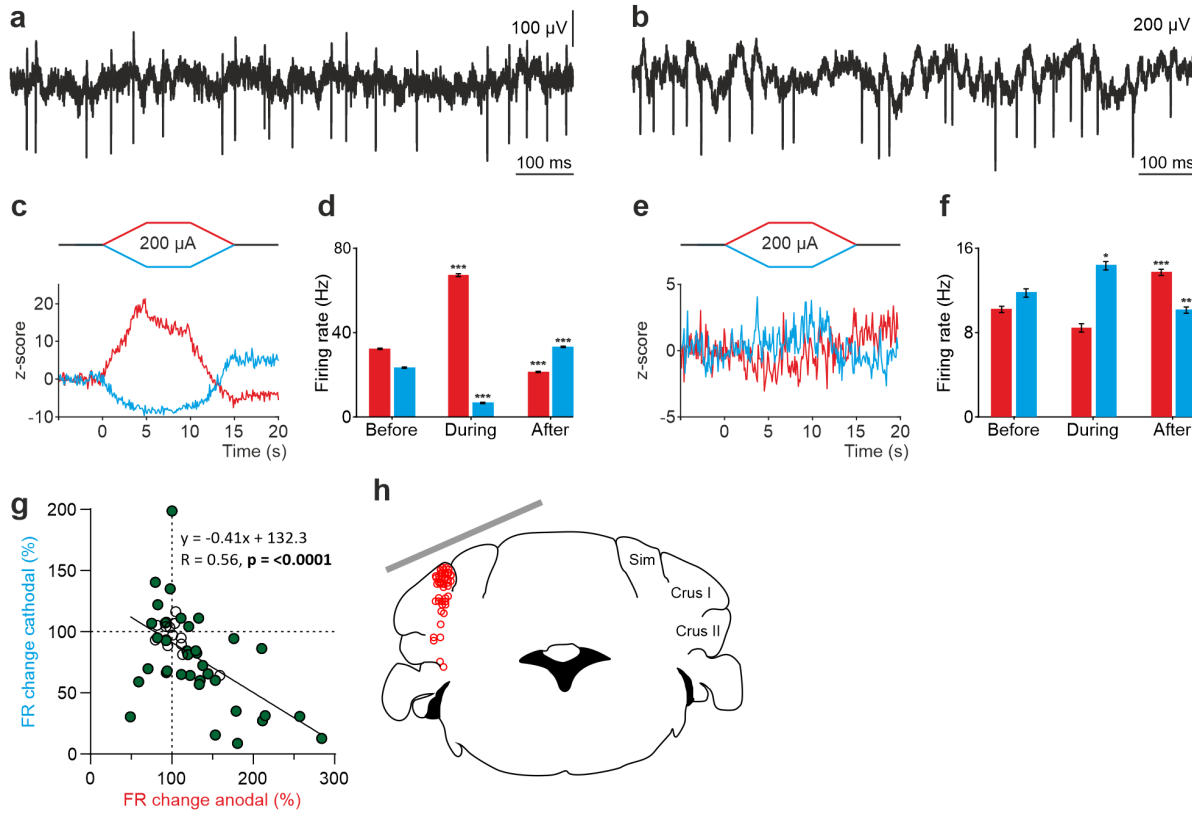

Fig. 3 tDCS modulation of non-PC activity in the awake mice. a, b Recording of spontaneous firing activity of two non-PC. **c, e** Z-score-transformed average PSTH (bin size: 0.1 s) of spontaneous spiking activity before, during and after anodal (red trace) or cathodal (blue trace) tDCS. **d, f** Statistical comparison of the firing rate between 5 s windows before, during and after tDCS (RM-ANOVA or Friedman tests, $p < 0.05$). Error bars represent SEM. *$p < 0.05$; **$p < 0.01$; ***$p < 0.001$. **g** Modulation of firing rate of individual neurons (circles) during anodal (red) and cathodal (blue) tDCS. Filled circles represent statistically significant modulation during tDCS (n = 50, RM-ANOVA or Friedman tests, $p < 0.05$). **h** Schematic representation of the recording sites and active electrode (gray bar) location during tDCS.

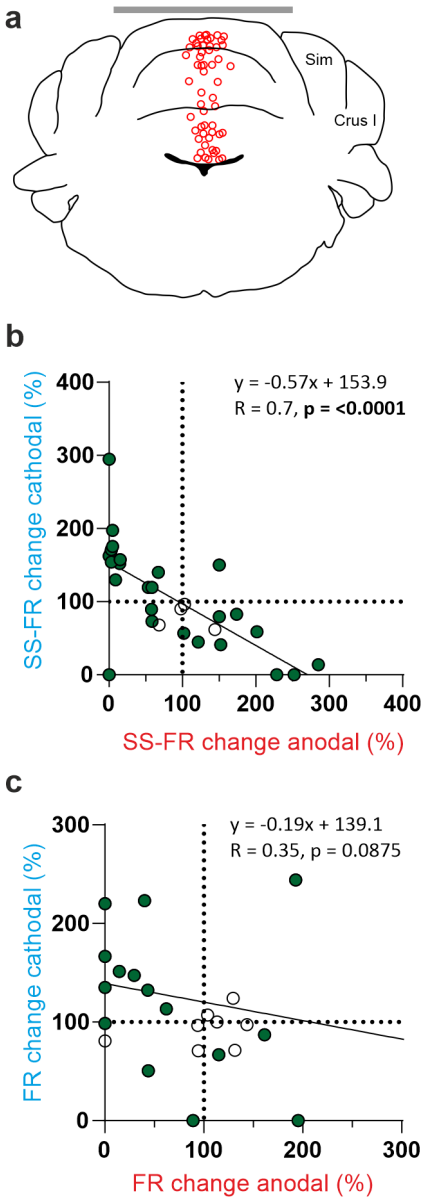

Fig. 4 tDCS modulation of PC and non-PC activity in anesthetized mice. a Schematic representation of the recording sites and active electrode (gray bar) location during tDCS. **b,c** Modulation of SS firing rate of individual PC (b) and firing rate of individual non-PC (c) during anodal (red) and cathodal (blue) tDCS over cerebellar vermis. Filled circles represent statistically significant modulation during tDCS (n = 31 PCs and 25 non-PCs, RM-ANOVA or Friedman tests, $p < 0.05$).

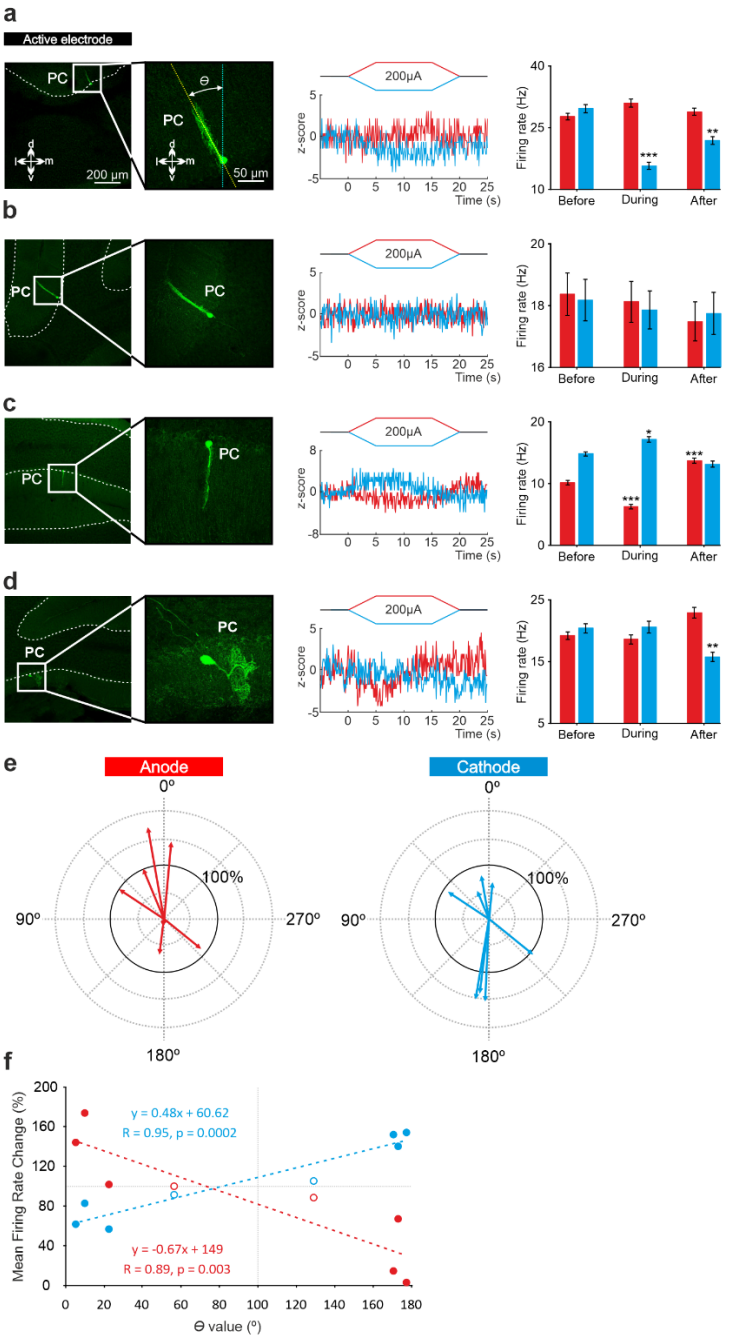

Fig. 5 Relationship between tDCS effects on PC and somatodendritic axis orientation in the anesthetized mice. a-d Confocal images of labeled neurons with different somatodendritic angles, z-score of their firing rate modulation during tDCS and statistical analysis (RM-ANOVA or Friedman tests, $p < 0.05$). Error bars represent SEM. *$p < 0.05$; **$p < 0.01$; ***$p < 0.001$. **e** Schematic representation of the firing rate modulation and the somatodendritic axis orientation with respect to the active electrode (θ, angle between the neuronal axis and an imaginary line perpendicular to the active electrode). Arrows length represents firing rate modulation during anodal (red arrows, at left) or cathodal (blue arrows, at right) tDCS at 200 µA with respect firing rate during control condition (represented by 100% solid circle). **f** Relationship between the averaged firing rate change value for anodal (red) and cathodal (blue) tDCS on each individual neuron with respect to its corresponding somatodendritic axis.

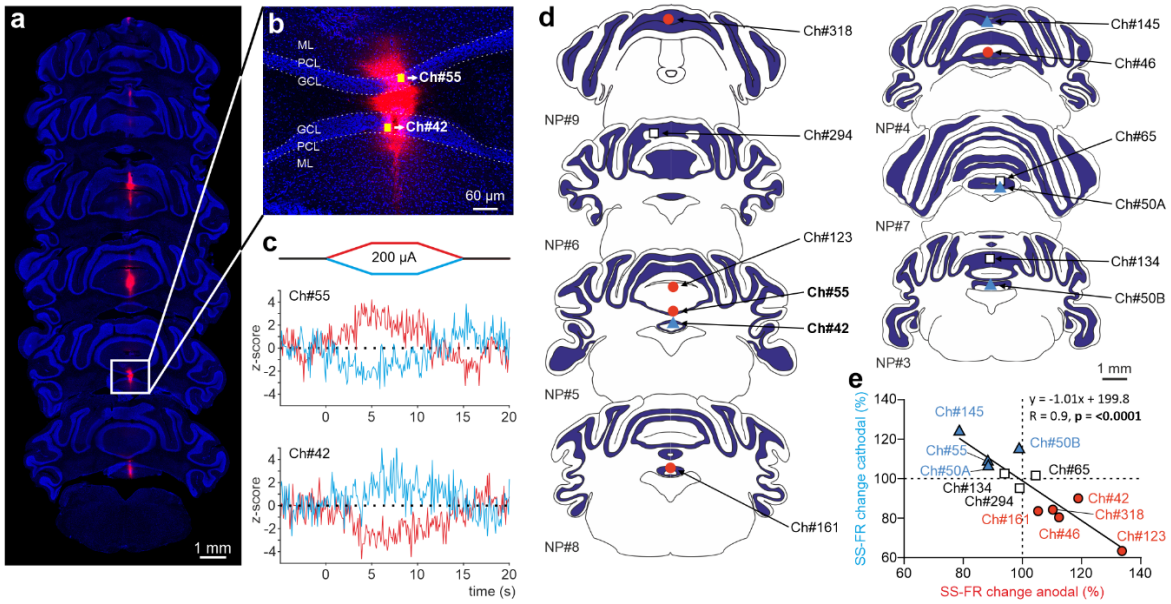

Fig. 6 tDCS effects on PCs simultaneously recorded at different PC layers in the awake mice. a Probe location marked with DiI in the cerebellar vermis stained with Hoechst 33342 dye. **b** Magnification of square area in "*a*" showing the theoretical location of two oppositely oriented PCs recorded at Ch#55 and Ch#42. **c** Z-score-transformed average PSTH (bin size: 0.1 s for SS) of the spontaneous SS before, during and after anodal and cathodal tDCS pulses for each simultaneously recorded PCs in one of the animals. **d** Anatomical localization of the different PC recorded. **e** Modulation of SS firing rate of individual PCs during anodal and cathodal tDCS. Filled symbols represent statistically significant modulation during tDCS (n = 12, RM-ANOVA or Friedman tests, $p < 0.05$). ML: molecular layer, PCL: Purkinje cell layer, GCL: granular cell layer.